HHS Public Access

Author manuscript

Cell Rep. Author manuscript; available in PMC 2024 April 16.

Published in final edited form as:

Cell Rep. 2024 March 26; 43(3): 113899. doi:10.1016/j.celrep.2024.113899.

LPD-3 as a megaprotein brake for aging and insulin-mTOR signaling in *C. elegans*

Taruna Pandey[1], **Bingying Wang**[1], **Changnan Wang**[1], **Jenny Zu**[1], **Huichao Deng**[2], **Kang Shen**[2], **Goncalo Dias do Vale**[3], **Jeffrey G. McDonald**[3], **Dengke K. Ma**[1,4,5,*]

[1]Cardiovascular Research Institute and Department of Physiology, University of California San Francisco, San Francisco, CA, USA

[2]Department of Biology, Howard Hughes Medical Institute, Stanford University, Stanford, CA, USA

[3]Center for Human Nutrition and Department of Molecular Genetics, University of Texas Southwestern Medical Center, Dallas, TX, USA

[4]Innovative Genomics Institute, University of California, Berkeley, Berkeley, CA, USA

[5]Lead contact

Abstract

Insulin-mechanistic target of rapamycin (mTOR) signaling drives anabolic growth during organismal development; its late-life dysregulation contributes to aging and limits lifespans. Age-related regulatory mechanisms and functional consequences of insulin-mTOR remain incompletely understood. Here, we identify LPD-3 as a megaprotein that orchestrates the tempo of insulin-mTOR signaling during *C. elegans* aging. We find that an agonist insulin, INS-7, is drastically overproduced from early life and shortens lifespan in *lpd-3* mutants. LPD-3 forms a bridge-like tunnel megaprotein to facilitate non-vesicular cellular lipid trafficking. Lipidomic profiling reveals increased hexaceramide species in *lpd-3* mutants, accompanied by up-regulation of hexaceramide biosynthetic enzymes, including HYL-1. Reducing the abundance of HYL-1, insulin receptor/DAF-2 or mTOR/LET-363, normalizes INS-7 levels and rescues the lifespan of *lpd-3* mutants. LPD-3 antagonizes SINH-1, a key mTORC2 component, and decreases expression with age. We propose that LPD-3 acts as a megaprotein brake for organismal aging and that its age-dependent decline restricts lifespan through the sphingolipid-hexaceramide and insulin-mTOR pathways.

Graphical abstract

*Correspondence: dengke.ma@ucsf.edu.

AUTHOR CONTRIBUTIONS

T.P., B.W., C.W., J.Z., and D.K.M. designed, performed, and analyzed most of the *C. elegans* experiments, contributed to project conceptualization, and wrote the manuscript. G.D.d.V. and J.G.M. contributed to lipid analysis. H.D. and K.S. contributed to the CRISPR allele generation and project conceptualization. D.K.M. supervised the project.

SUPPLEMENTAL INFORMATION

Supplemental information can be found online at https://doi.org/10.1016/j.celrep.2024.113899.

DECLARATION OF INTERESTS

The authors declare no competing interests.

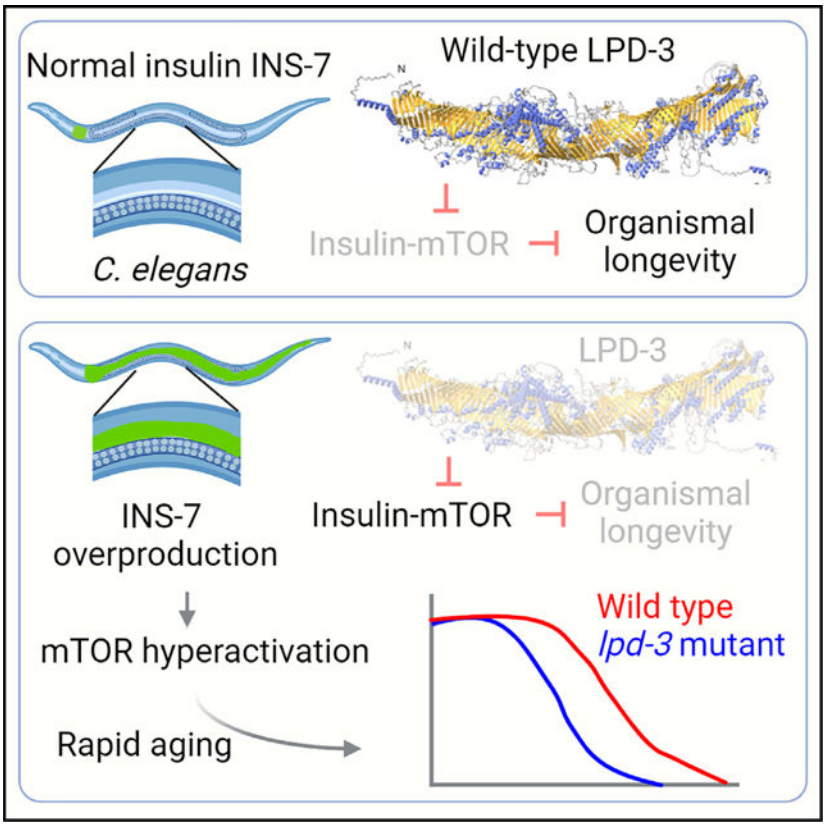

In brief

Pandey et al. identify LPD-3, a bridge-like lipid transfer protein, as a megaprotein "brake" critical for preventing insulin-mTOR hyperfunction during *C. elegans* aging. The underlying mechanism involves LPD-3's orchestration of the rheostat balance between the phospholipid and hexaceramide species that regulate *C. elegans* lifespan through the insulin-mTORC2 and mitochondrial pathways.

INTRODUCTION

Organismal aging occurs pervasively in nature. Numerous theoretical and empirical studies have sought to address how aging evolves at the species population level and how an organism ages at the mechanistic level. Evolutionary theories of aging have provided useful frameworks for understanding why organisms age in various species, emphasizing the importance of declining natural selection forces post-organismal reproduction.[1–3] Nonetheless, what biological processes may cause aging at the mechanistic level remains a contentious unresolved question, despite many well-defined and characterized "hallmarks" associated with aging.[4–6] Major mechanistic theories of aging, including the molecular damage and mutation accumulation (MA) theory and the hyperfunction and antagonistic pleiotropy (AP) theory of aging, have stimulated many studies to test predictions from each.[7–14] While the MA theory highlights the critical roles of molecular damages incurred over time during aging, the AP and hyperfunction theory posits that key anabolic processes

keep running post-reproduction and/or become abnormally hyperactivated and thereby cause aging and age-related pathologies.[7–9] Such AP effects are features of several cellular anabolic signaling proteins, including insulin and mTOR (mechanistic target of rapamycin). Late-life dysregulation or hyperfunction of insulin-mTOR signaling can indeed contribute to aging and age-associated pathologies, including type 2 diabetes, cardiovascular diseases, and cancer.[15–17]

The discovery of exceptionally long-lived mutants in *C. elegans* has ushered in a transformative era in aging research, leveraging the genetic tractability of this model organism well suited for aging studies.[18–21] Reduced abundance or activity in components of the insulin pathway (the insulin receptor DAF-2 or the PI-3 kinase AGE-1) extends longevity through mechanisms that have been extensively studied and involve, at least in part, activation of geroprotective transcription factors, including DAF-16 (foxO ortholog), HSF-1 (heat shock factor-1), and SKN-1 (mammalian Nrf-2 ortholog).[22–24] The insulin-PI-3 kinase pathway promotes anabolic growth and reproduction in coordination with mTOR signaling, inhibition of which can extend lifespan and longevity in phylogenetically diverse eukaryotic organisms. While such loss-of-function models have been highly valuable and support critical roles of insulin-mTOR in aging from diverse multicellular organisms, whether and how insulin-mTOR hyperfunction may actively drive aging and age-associated pathological phenotypes remain underexplored. Downstream of insulin or growth factor signaling, many mTOR regulators have been identified, including the TSC1-TSC2 (tuberous sclerosis proteins) complex as a critical negative regulator of mTORC1 activation.[25] However, the absence of apparent homologs of TSC in the *C. elegans* genome suggests that previously unknown regulators upstream of insulin-mTOR signaling may still elude identification. These unidentified factors could play a crucial role in preventing insulin-mTOR hyperfunction and regulating the pace of aging.

In recent studies, we identified *lpd-3* (lipid depleted) in a mutagenesis screen and discovered that the 452 kDa megaprotein LPD-3 acts as a bridge-like lipid-transfer protein (BLTP) with evolutionarily conserved roles in phospholipid trafficking from the endoplasmic reticulum (ER) to plasma membranes (PMs) (Figure 1A).[26–28] Mutations in *BLTP1*, the human ortholog of *lpd-3*, cause an autosomal recessive genetic disorder, Alkuraya-Kučinskas syndrome (AKS).[29–31] Since most AKS patients die prematurely of unknown etiology, we sought to determine the lifespan of *lpd-3* mutants and explore how LPD-3 deficiency may cause AKS-related pathologies in *C. elegans*. Through combined genetic, lipidomic, and phenotypic analyses, our results reveal the critical roles of LPD-3 in organismal resilience and longevity, linking phospholipid-sphingolipid balance, insulin-mTOR hyperfunction, and mitochondrial regulation to the tempo modulation of aging.

RESULTS

LPD-3 regulates normal lifespan through INS-7

To determine how LPD-3 deficiency may affect aging, we generated two backcrossed strains carrying a deletion allele, *ok2138*, or a CRISPR-generated stop-codon allele, *wy1772*, respectively, and performed lifespan analysis in these two strains as compared to wild type (Figure 1B). We found that both strains showed strikingly shortened lifespans at

the three common temperature cultivation conditions tested (Figures 1C–1E; Table S1). Thereafter, we used the *lpd-3* deletion allele *ok2138* to investigate the role of *lpd-3* in lifespan regulation in comparison to wild type. In addition to shortened median and maximal lifespans, we found that *lpd-3* mutants exhibited various common aging phenotypes, including age pigment and reduced behavioral locomotion, that occurred markedly earlier than in wild-type animals (Figure S1). The exceptionally large size of *lpd-3* cDNA prevented us from successfully obtaining a lifespan-rescuing transgene. Nonetheless, similar phenotypes of both alleles of *lpd-3* that we have extensively backcrossed (>5 generations), as well as the comparable lifespan-shortening effect of RNAi against *lpd-3* (Table S1), support the causal role of LPD-3 in ensuring normal lifespan and longevity in *C. elegans*.

The drastically shortened lifespan of *lpd-3* mutants prompted us to determine the underlying mechanisms. By analyzing RNA sequencing (RNA-seq) datasets for *lpd-3* mutants compared with wild type,[26] we discovered that LPD-3 deficiency led to a nearly 40-fold increase in the expression level of *ins-7* (Figure 1F), which represents one of the most highly *lpd-3* up-regulated genes and encodes an agonist insulin with previously reported effects on aging and lifespan in *C. elegans*.[32–34] Expression of other insulin-encoding genes was much less regulated or was largely unaltered (Figures S2A and S2B). To determine the spatiotemporal site of *ins-7* regulation, we crossed an integrated *ins-7*p::INS-7::GFP translational reporter strain[35] with the *lpd-3*(*ok2138*) deletion mutant. In the wild type, *ins-7*p::INS-7::GFP is expressed at baseline levels that are detectable only in the anterior part of the intestine at 15°C starting from young adult stages (24 h post-L4, or fourth larval stage) and increased at 20°C and 25°C (Figure 1G). By contrast, *ins-7*p::INS-7::GFP in *lpd-3* mutants showed drastically increased INS-7::GFP abundance and fluorescence throughout the intestine particularly under higher temperatures (20°C or 25°C). We showed previously that *lpd-3* mutants are defective in ER-to-PM phospholipid trafficking and that they exhibit sensitivity to thermal stress that can be normalized by lecithin.[26] We confirmed in this study that lecithin supplementation in the culture medium rescued both the shortened lifespan and *ins-7*p::INS-7::GFP up-regulation phenotypes (Figures S2C and S2D). High-resolution confocal imaging revealed the *in vivo* location and subcellular distribution of the massive up-regulated INS-7::GFP reporter signal predominantly in the intestine of *lpd-3* mutants (Figures S2E and S2F), suggesting a cell-autonomous-specific regulation of *ins-7* by LPD-3, which acts in the intestine to facilitate ER-to-PM lipid trafficking.[26]

To determine the causal role of *ins-7* in the shortened lifespan phenotype of *lpd-3* mutants, we used RNAi to knock down *ins-7* expression in *lpd-3* mutants. We found that treatment with RNAi against *ins-7* led to a markedly extended lifespan of *lpd-3* mutants comparable to that in the wild type (Figure 1H). We also observed such rescue of the shortened lifespan of *lpd-3* mutants by RNAi against *daf-2* (Figure 1I), which encodes the only known receptor of insulin in *C. elegans*. We note that control RNAi also led to a slight increase in lifespan in *lpd-3* mutants (Figures 1D and 1H), likely reflecting different lipid compositions of *E. coli* strains between OP50 and HT115 strains[36,37] used in routine *C. elegans* culture and RNAi experiments, respectively. Reducing *ins-7* expression has been previously shown to increase the lifespan of wild-type animals, implicating INS-7's role in tissue entrainment by feedback regulation with its receptor DAF-2 and the downstream transcription factor DAF-16 in *C. elegans*.[32–34] Our results support these early findings and further reveal that

INS-7 overproduction is causally responsible for shortening the lifespan of *lpd-3* mutants, in a manner that requires the sole insulin receptor DAF-2 (Figure 1J).

Roles of mTOR and sphingolipids in INS-7 up-regulation in *lpd*-3 mutants

We aimed to determine the regulatory mechanisms leading to *ins-7* up-regulation and shortened lifespan in *lpd-3* mutants. Taking advantage of the drastically up-regulated *ins-7*p::INS-7::GFP reporter in *lpd-3* mutants as a live fluorescent readout, we performed targeted RNAi screens to identify genes required for *ins-7*p::INS-7::GFP up-regulation by *lpd-3*. We performed RNAi for those genes with reported adequate expression in the intestine (transcript per million > 2) and encoding mediators of major signal transduction pathways known to be involved in insulin signaling (the Ras/MAPK, phospholipase, and PI3 kinase/mTORC1/mTORC2 pathways)[38–40] (Table S2). As positive controls, we verified the strong effects of *ins-7* or *daf-2* RNAi in suppressing *ins-7*p::INS-7::GFP expression in *lpd-3* mutants (Figures 2A and 2B). From such screens, we found that RNAi against several genes encoding components of the mTORC2 complex in *C. elegans*, including *let-363* (orthlog of human MTOR), *rict-1* (RICTOR ortholog), and *sinh-1* (otholog of SIN-1/human MAPK associated protein 1), led to a marked reduction of *ins-7*p::INS-7::GFP in *lpd-3* mutants (Figures 2A–2C). RNAi against genes involved in the mTORC1 complex, except *let-363*, shared by mTORC1 and mTORC2, exhibited weaker effects (Figure 2A).

In parallel to such RNAi screens, we also performed lipidomic profiling of *lpd-3* mutants compared to the wild type since LPD-3 normally functions as a BLTP.[26] Among all major lipid species examined by liquid chromatography-tandem mass spectrometry, including phospholipids, glycerolipids, and sphingolipids (Table S3), the hexaceramide type of sphingolipids showed marked up-regulation in *lpd-3* mutants (Figure 2D). Consistently, RNA-seq results revealed that genes encoding hexaceramide biosynthetic enzymes (Figure 2E), including HYL-1 and CGT-1/2/3, were markedly up-regulated in *lpd-3* mutants (Figure 2F). As reduced LPD-3 activity results in impaired ER-to-PM phospholipid trafficking, a lipid homeostatic mechanism is likely triggered to up-regulate sphingolipids in *lpd-3* mutants.[26] Given reported sphingolipid modulation of mTOR signaling and longevity,[41–43] we next explored the link of hexaceramide biosynthetic enzyme HYL-1 to *ins-7*. We found that *hyl-1* RNAi led to a strong suppression of *ins-7*p::INS-7::GFP in *lpd-3* mutants (Figure 2B). Functionally, lifespan analysis revealed that RNAi against *rict-1* or *hyl-1* led to marked rescue of the shortened lifespan in *lpd-3* mutants (Figures 2G and 2H). RNAi against *sgk-1* (serum and glucocorticoid inducible kinase-1 ortholog), which encodes a major downstream kinase[44–46] mediating effects of mTORC2, showed similar rescuing effects (Figure 2I). Taken together, these results indicate that the sphingolipid-mTOR pathway drives *ins-7* overexpression, leading to the shortened lifespan in *lpd-3* mutants.

We next explored cellular mechanisms by which LPD-3 regulates mTORC2. The mTORC2 complex in *C. elegans* consists of the core subunit LET-363 shared by mTORC1 and the mTORC2-specific subunits RICT-1 and SINH-1 (Figure 3A). As the mammalian homologs of SINH-1 bind to PIP3 at the PM and mediate signaling from insulin receptors to the mTORC2 complex,[16,47,48] we tagged endogenous SINH-1 with GFP by CRISPR (Figure 3B) and monitored how LPD-3 may affect the intracellular abundance and localization of

SINH-1::GFP. In the wild type, we did not observe apparent SINH-1::GFP fluorescence throughout animals at the young adult stage (24 h post-L4). By contrast, RNAi against *lpd-3* or its mutations led to a marked increase of SINH-1::GFP fluorescence signals that were particularly enriched at loci near PM in the intestine (Figures 3C and 3D). As expected, RNAi against *lpd-3* also effectively decreased the abundance of LPD-3 endogenously labeled with GFP by CRISPR (Figure 3E, and see below). Since the loss of LPD-3 causes PIP2/3 to accumulate in the ER membrane near the ER-PM junction,[26] increased SINH-1::GFP in *lpd-3* mutants likely reflects its ectopic intracellular activity. In addition to the *ins-7* phenotype (Figure 2), we found that *lpd-3* mutants exhibited morphologically spherical (i.e., abnormally swollen) mitochondria with decreased branch lengths, whereas RNAi against genes encoding the mitochondrial fission machinery (DRP-1, dynamin related protein-1) or insulin-mTOR pathway components (INS-7, DAF-2, SINH-1, SGK-1) strongly suppressed such phenotypes (Figures 3F and 3G). These results are consistent with emerging roles of mTORC2 in regulating mitochondria[49–51] and, further, indicate that LPD-3 normally functions to restrict the accumulation of SINH-1, a mTORC2 component, and thereby antagonize ectopic mTOR activity.

We assessed the effect of mitochondrial abnormalities on molecular damage through reactive oxygen species (ROS) generation by employing the MitoTracker Red CM-H2Xros staining method on wild type and *lpd-3*(*ok2138*) mutants. MitoTracker Red CM-H2Xros fluorescence, indicative of mitochondrial-specific ROS,[52] revealed a markedly higher level in *lpd-3* mutants compared to the control (Figure S3A). Treatment with the mitochondrial ROS scavenger mito-TEMPO (a superoxide dismutase mimetic)[53,54] partially rescued the increased ROS and shortened lifespan phenotypes in *lpd-3* mutants (Figures S3B and S3C). Excessive ROS generated from the mitochondria can contribute to the initiation and perpetuation of the vicious iron cycle, playing a pivotal role in the progressive accumulation of cellular damage.[55,56] Consistently, we observed strong up-regulation of the *ftn-1* transcriptional reporter and increased ferroOrange staining of the labile iron pool in *lpd-3* mutants (Figures S3D and S3E). We note the caveat that mito-TEMPO, with its inadequate absorption in tissues other than the intestine and its likely short half-life *in vivo*, undermines its full effect in lifespan rescue. It also remains to be determined at which dose mito-TEMPO can mitigate the molecular damaging effects of ROS while still allowing potential hormetic effects of ROS on lifespan modulation. Nonetheless, these findings suggest that mitochondrial phenotypes caused by insulin-mTOR hyperactivity in *lpd-3* mutants may lead to mitochondrial dysfunction and iron overload, likely contributing to their accelerated aging phenotype.

Regulation and functional roles of LPD-3 during aging of wild-type animals

Are endogenous LPD-3 abundance and activity subject to regulation by normal aging in wild-type animals? To address this question, we tagged endogenous LPD-3 with seven copies of the split GFP (GFP11) by CRISPR[57–59] and crossed the allele into a strain expressing GFP10 specifically in the intestine by the *ges-1* promoter (Figure 4A). We monitored how aging affects the intracellular abundance and localization of LPD-3::GFP based on the complementation of GFP1–10 and 7xGFP11 in the intestine, the site of which we showed previously is critical for LPD-3 functions in phospholipid trafficking.[26] Confocal

microscopy revealed that LPD-3::GFP is enriched along the apical membrane of the intestine at the L4 and young adult stages, with an age-dependent progressive decline in abundance at the stages of days 3, 5, and 9 (Figures 4B and 4C). Functionally, we showed previously that LPD-3 facilitates ER-to-PM trafficking of phospholipids, including phosphatidylcholine and phosphatidylinositol. Using Akt-PH::GFP, which binds to the phosphatidylinositol species PIP2/PIP3, we found that aging caused a progressive decline of Akt-PH::GFP signals at the intestinal apical membrane, while *lpd-3* loss-of-function mutations exacerbated such age-dependent decline (Figures 4D and 4E). By contrast, *ins-7*p::INS-7::GFP exhibited an age-dependent increase in abundance, while such age-dependent change was accelerated in *lpd-3* mutants (Figures 4F and 4G). These results demonstrate the age-dependent decline in both the abundance and functional activity of endogenous LPD-3 during normal *C. elegans* aging.

DISCUSSION

In this study, we provide multiple lines of evidence to support the specific role of insulin-mTOR in causing the shortened lifespan of *lpd-3* mutants. First, gene expression profiles from RNA-seq results of wild type and *lpd-3* mutants identified dramatic and specific up-regulation (approximately 40-fold increase) of *ins-7*, which was confirmed by the *ins-7*p::INS-7::GFP translational reporter, in *lpd-3* mutants (Figures 1; S2). Our studies revealed gene expression patterns and aging characteristics consistent with the hyperactivation of insulin-mTOR as opposed to translational inhibition or bioenergetic failure, which are indicative of a general state of illness. Second, employing RNAi against genes encoding INS-7 or its activating receptor DAF-2, we show that the elevated levels of *ins-7* and DAF-2 are causally linked to the reduced lifespan of *lpd-3* mutants. Although previous studies and our confirmatory findings (Figure S4) indicate that the loss of INS-7 or DAF-2 can extend the lifespan of wild-type animals, these results do not conflict with our conclusions regarding *lpd-3* mutants. Instead, the up-regulation of *ins-7* and the extension of lifespan through *ins-7* RNAi in *lpd-3* mutants point to a specific regulatory mechanism by which LPD-3 influences aging rather than a general state of compromised health. Third, our evidence indicates that insulin-mTOR hyperactivation may shorten lifespan, possibly through mitochondrial dysfunction and iron overload (Figure S3). Taken together, these results support a specific molecular cascade leading to a shortened lifespan of *lpd-3* mutants.

Identification and subsequent mechanistic studies of exceptionally long-lived *C. elegans* mutants in the insulin-mTOR pathway have provided crucial insights into how the loss of insulin-mTOR function extends longevity. Activation of key transcription factors including DAF-16, HSF-1, and SKN-1 mediates geroprotective effects in these mutants by promoting somatic maintenance programs that may attenuate molecular and cellular damages. Our studies provide a complementary model in which insulin overproduction and mTOR hyperfunction can actively drive aging downstream of LPD-3 and the sphingolipid-ceramide pathway (Figure S4). Our findings support the notion that somatic maintenance programs and molecular/cellular damaging agents (e.g., excess ROS, iron, and/or cell death-triggering signals) from dysregulated mitochondria may converge to control the tempo of aging downstream of insulin-mTOR. Based on new insights from *C. elegans* models, this view

may imply reconciling and unifying the two prevalent mechanistic theories of aging (molecular damage versus mTOR hyperfunction).[7–14]

Various sphingolipids have been shown to contribute to organismal aging and age-associated pathologies.[60–62] We identify LPD-3 as a critical megaprotein regulator of the phospholipid-sphingolipid balance or rheostat, dysfunction of which can impact aging via insulin-mTOR hyperfunction. LPD-3 defines a member of a recently discovered and highly evolutionarily conserved protein family that controls lipid homeostasis in eukaryotic cell membranes.[26,28,63,64] Based on our findings and prior studies supporting emerging roles of sphingolipid/ceramides and conserved insulin-mTOR signaling from many species,[3,42,61,62,65] we propose that LPD-3 may act as a cellular brake that slows organismal aging by orchestrating its tempo and regulating the sphingolipid-insulin-mTOR axis, likely in phylogenetically diverse organisms.

Limitations of the study

Limitations of the study include the incompletely defined signaling, transcriptional, and epigenetic regulatory mechanisms linking LPD-3 to sphingolipid regulation, insulin overproduction, and lifespan, which await further studies. We employed mostly genetic, lifespan phenotypic, transcriptomic, and lipidomic approaches, which cannot resolve remaining interesting biochemical questions, including the ceramide-type specificity involved in aging regulation. Whether the gain of function of *lpd-3* can extend longevity in *C. elegans* and whether LPD-3 homologs play evolutionarily conserved roles in lifespan regulation in other organisms remain to be determined. The study was prompted by the clinical phenotype of patients with AKS who experience early mortality, yet the causal link of insulin-mTOR to AKS remains unclear. In addition, the genetic deletion and stop codon mutations of *lpd-3* do not represent null alleles and might not entirely abolish gene function due to potential alternative splicing, and using reduction-of-function non-null alleles or RNAi precludes strict conclusions on epistasis relationships among the genes studied.

STAR★METHODS

RESOURCE AVAILABILITY

Lead contact—Further information and requests for resources and reagents should be directed to and will be fulfilled by the lead contact, Dengke K. Ma, Ph.D. (dengke.ma@ucsf.edu).

Materials availability—Most strains of the *Caenorhabditis* strains and isolates used in this study are available through *Caenorhabditis* Genetics Center (CGC). The strains/reagents generated in this study can be requested from the lead contact, Dengke K. Ma, Ph.D. (dengke.ma@ucsf.edu). All unique/stable reagents generated in this study are available from the lead contact without restriction.

Data and code availability

- The RNAseq read datasets were deposited in NCBI SRA (Sequence Read Archive) under the BioProject accession PRJNA827259. All other data generated for this study are included in this article.
- This paper does not report original code.
- Any additional information required to reanalyze the data reported in this paper is available from the lead contact upon request.

EXPERIMENTAL MODEL AND STUDY PARTICIPANT DETAILS

Strain culture and maintenance—All *C. elegans* strains were kept at 20°C for both maintenance and experiments unless otherwise specified. All *C. elegans* strains were non-starved for at least 2 generations on NGM plates seeded with OP50 bacteria before experiments. The details of each strain are listed in the key resources table. The *E. coli* strain HT115 (DE3) was obtained from the Ahringer RNAi library. *daf-2* and *sgk-1* RNAi clones were generated in this study using L4440 as the vector backbone and *daf-2 and sgk-1* coding sequences as the inserts (sequence listed in key resource table). All RNAi clones were verified by PCR and restriction digestion. RNAi strains were cultured for 16 h in LB with 1 mM ampicillin, and then seeded onto RNAi NGM plates that contain 1 mM IPTG and 1 mM ampicillin. The RNAi bacteria-seeded plates were then left at room temperature overnight for induction of dsRNA expression. Lecithin and mito-TEMPO were dissolved in distilled water and were supplemented to the NGM plate surface for compound exposure from the embryo stage.

METHOD DETAILS

Lifespan assessment—The wild type N2 and other strains of indicated genotypes and conditions were grown for two generations without starvation, and then embryos were synchronized through sodium hypochlorite (4%) and sodium hydroxide (5 M) treatment. The embryos were washed three times with M9. These embryos were grown on OP50-seeded plates or transferred to RNAi-seeded NGM plates. Thereafter, late-L4 larvae or young adults (24 h post-L4) were transferred to OP50-seeded plates or RNAi-seeded NGM plates supplemented with 50 μM of 5-fluoro-2-deoxyuridine (FUDR, Sigma) to prevent progeny growth. Assay populations were transferred to fresh OP50-seeded plate every 3–4 days. Live/dead/missing worms were scored on alternate days until the last surviving worm. The live worms were detected through touch-provoke responses. The lifespan assays were repeated for at least 40–70 worms in three independent trials (Table S1).

Epifluorescence and confocal microscopic imaging—The epifluorescence compound (Leica DM5000B), confocal microscopes (Leica DM6) and laser scanning confocal FV3000 (Olympus, US) were used to capture confocal fluorescence images. Animals of various genotypes or treated with different RNAi or compounds (Lecithin, mito-TEMPO) were randomly picked at synchronized stages (24 h post L4) and treated with 10 mM sodium azide in M9 solution (Sigma-Aldrich), symmetrically aligned on 2% agar pads on slides for imaging and covered with coverslip. The control and treatment groups were imaged under identical settings and conditions unless otherwise mentioned.

The epifluorescence compound (Leica) microscope was used to measure the mean fluorescence of *ins-7p::ins-7::gfp* and *ins-7p::ins-7::gfp; lpd-3(ok2138)* at different temperatures (20°C, 25°C and 15°C) and time points (day 1, 5 and 10). For RNAi or compound treatment (Lecithin 20 mg/mL), worms were exposed from synchronized stages of embryos and imaged on day 2 post L4. The quantification of the GFP reporters was scored as mean fluorescence. The age-dependent decline in LPD-3:GFP, AKT(PH):GFP and AKT(PH):GFP*; lpd-3(ok2138)* strains were scored by calculating the mean fluorescence value from the z stack of confocal planes in each worm at different time point near the apical membrane using the ImageJ software.

The penetrance of SINH-1:GFP post RNAi treatment was scored as a percentage of animals that exhibit detectable fluorescence near the apical membrane localization in z stack of confocal planes. For detection of mitochondrial morphology aberration in wild-type *mai-2*::GFP and *mai-2*::GFP; *lpd-3(ok2138)* treated with RNAis, confocal images were scored based on mitochondrial morphology. The aberrant mitochondrial morphology was identified as spherical mitochondria with respect to normal rod-shaped mitochondria. Then, the percentage of spherical mitochondria was plotted in each image and counted manually for quantification.

MITOCHONDRIAL ROS AND CELLULAR IRON IMAGING

FerroOrange (Dojindo, F374–10) was used to measure levels of intracellular free iron pools in wild type and *lpd-3(ok2138)* mutants. The stock solution of Ferrorange (1 mM) was dissolved in 35 μL DMSO with working solution of 10 μM made in M9. A synchronized worm population was obtained from sodium hypochlorite treatment and day 2 young adult worms (48 h post L4) were used for staining. The worms were washed with M9 and centrifuged at 1000 rpm, which was repeated three times to remove all the adherent OP50. Then, the worms exposed to 10 μM FerroOrange in M9 for 2 h with constant gentle shaking in the dark at room temperature. Before imaging, the worms were washed three times with M9. Imaging was done at 40X objective at excitation emission (540–600 nm). For mitochondrial ROS detection by MitoTracker, red CM-H2XRos (ThermoFisher Scientific) was used. The 1 mM stock solution was prepared by adding 100 μL DMSO in vials provided. Then, synchronized-stage worms of wild type and *lpd-3(ok2138)* with or without MitoTEMPO supplementation in NGM plates were transferred and incubated with the dye at working concentration 0.5 μM and imaged post overnight incubation at 20°C (excitation, emission: 560 nm, 600 nm). Quantification of mean fluorescence was conducted through ImageJ.

Behavioral and age pigment/age pigment measurements during aging—The locomotion of worms was measured using video acquired through the WormLab System. Worms at different stages were picked from NGM plate supplemented with OP50 to a fresh NGM plate without OP50 at 30 min before video acquisition. The speed (total track length/time) of age-synchronized worms recorded using the WormLab System was based on the midpoint positions of the worms. Each experiment was repeated three times with more than 10 animals per group. The age pigment analysis with age progression was measured by using ultraviolet light excitation coupled with detection through a blue/cyan filter with

confocal microscopy and quantified by calculating the mean fluorescence value in each worm using the ImageJ software.

Lipidomic analysis—Wild type N2 strain and *lpd-3*(*ok2138*) mutants were grown under non-starved conditions for four generations at 20°C, followed by bleach synchronization and harvest by M9 buffer at young adult stages. Frozen worm pellets (50 μL per sample, three independent biological replicates per genotype) are stored until lipidomic extraction and analysis. All solvents for lipidomic extraction and analysis used were either HPLC or LC/MS grade and purchased from Sigma-Aldrich (St Louis, MO, USA). Splash Lipidomix standards were purchased from Avanti (Alabaster, AL, USA). All lipid extractions were performed in 16 × 100mm glass tubes with PTFE-lined caps (Fisher Scientific, Pittsburg, PA, USA). Glass Pasteur pipettes and solvent-resistant plasticware pipette tips (Mettler-Toledo, Columbus, OH, USA) were used to minimize leaching of polymers and plasticizers. Samples were transferred to fresh glass tubes, and 1 mL of methanol, 1mL of water and 2mL of methyl *tert*-butyl ether (mTBE) were added for liquid-liquid extraction. The mixture was vortexed and centrifuged at 2,671 g for 5 min, resulting in two distinct liquid phases. The organic phase (upper phase) was transferred to a fresh tube with a Pasteur pipette and spiked with 20uL of a 1:5 diluted Splash Lipidomix standard mixture. The samples were dried under N_2 and resuspended in 400 μL of hexane. Lipids were analyzed by LC-MS/MS using an SCIEX QTRAP 6500$^+$ (SCIEX, Framing-ham, MA) equipped with a Shimadzu LC-30AD (Shimadzu, Columbia, MD) high-performance liquid chromatography (HPLC) system and a 150 × 2.1 mm, 5 μm Supelco Ascentis silica column (Supelco, Bellefonte, PA). Samples were injected at a flow rate of 0.3 mL/min at 2.5% solvent B (methyl *tert*-butyl ether) and 97.5% Solvent A (hexane). Solvent B was increased to 5% over 3 min and then to 60% over 6 min. Solvent B was decreased to 0% during 30 s while Solvent C (90:10 (v/v) isopropanol-water) was set at 20% and increased to 40% during the following 11 min. Solvent C is increased to 44% over 6 min and then to 60% over 50 s. The system was held at 60% solvent C for 1 min prior to re-equilibration at 2.5% of solvent B for 5 min at a 1.2 mL/min flow rate. Solvent D [95:5 (v/v) acetonitrile-water with 10 mM Ammonium acetate] was infused post-column at 0.03 mL/min. Column oven temperature was 25°C. Data was acquired in positive and negative ionization mode using multiple reaction monitoring (MRM). The LC-MS/MS data was analyzed using MultiQuant software (SCIEX). The identified lipid species were normalized to its corresponding internal standard.

QUANTIFICATION AND STATISTICAL ANALYSIS

All the data in the current manuscript were analyzed using GraphPad Prism 9.2.0 Software (Graphpad, San Diego, CA) and presented as means ± S.E.M. unless otherwise specified, with significance p values calculated by unpaired two-sided *t*-tests (comparisons between two groups), one-way or two-way ANOVA (comparisons across more than two groups) and adjusted with Bonferroni's multiple comparisons and Tukey HSD post hoc tests. Lifespan assay was quantified using Kaplan–Meier lifespan analysis and p values were calculated using the log rank test.

Supplementary Material

Refer to Web version on PubMed Central for supplementary material.

ACKNOWLEDGMENTS

Some strains were provided by Dr. Yun Zhang's group at Harvard University, Dr. R.E. Navarro's group at Universidad Nacional Autónoma de México, and by the *Caenorhabditis* Genetics Center (CGC), which is funded by NIH Office of Research Infrastructure Programs (P40 OD010440). C.W. was supported by NSF of China (31971077) and the Shanghai Pujiang Program (23PJ1403300). The work was financially supported by the NIH/NIGMS grant 1R35GM139618, UCSF PBBR New Frontier Research, and UCSF BARI Investigator Award (D.K.M.).

REFERENCES

1. Gavrilov LA, and Gavrilova NS (2002). Evolutionary Theories of Aging and Longevity. Sci. World J 2, 339–356. 10.1100/tsw.2002.96.
2. Flatt T, and Partridge L (2018). Horizons in the evolution of aging. BMC Biol. 16, 93. 10.1186/s12915-018-0562-z. [PubMed: 30124168]
3. Pandey T, and Ma DK (2022). Stress-Induced Phenoptosis: Mechanistic Insights and Evolutionary Implications. Biochemistry 87, 1504–1511. 10.1134/S0006297922120082. [PubMed: 36717459]
4. Blagosklonny MV (2022). Hallmarks of cancer and hallmarks of aging. Aging (Albany NY) 14, 4176–4187. 10.18632/aging.204082. [PubMed: 35533376]
5. López-Otín C, Blasco MA, Partridge L, Serrano M, and Kroemer G (2013). The Hallmarks of Aging. Cell 153, 1194–1217. 10.1016/j.cell.2013.05.039. [PubMed: 23746838]
6. Schmauck-Medina T, Molière A, Lautrup S, Zhang J, Chlopicki S, Madsen HB, Cao S, Soendenbroe C, Mansell E, Vestergaard MB, et al. (2022). New hallmarks of ageing: a 2022 Copenhagen ageing meeting summary. Aging (Albany NY) 14, 6829–6839. 10.18632/aging.204248. [PubMed: 36040386]
7. Blagosklonny MV (2006). Aging and immortality: quasi-programmed senescence and its pharmacologic inhibition. Cell Cycle 5, 2087–2102. 10.4161/cc.5.18.3288. [PubMed: 17012837]
8. Blagosklonny MV (2021). The hyperfunction theory of aging: three common misconceptions. Oncoscience 8, 103–107. 10.18632/oncoscience.545. [PubMed: 34549076]
9. Gems D (2022). The hyperfunction theory: An emerging paradigm for the biology of aging. Ageing Res. Rev 74, 101557. 10.1016/j.arr.2021.101557. [PubMed: 34990845]
10. Gladyshev VN (2016). Aging: progressive decline in fitness due to the rising deleteriome adjusted by genetic, environmental, and stochastic processes. Aging Cell 15, 594–602. 10.1111/acel.12480. [PubMed: 27060562]
11. Longo VD, Mitteldorf J, and Skulachev VP (2005). Programmed and altruistic ageing. Nat. Rev. Genet 6, 866–872. 10.1038/nrg1706. [PubMed: 16304601]
12. de Magalhães JP, and Church GM (2005). Genomes optimize reproduction: aging as a consequence of the developmental program. Physiology 20, 252–259. 10.1152/physiol.00010.2005. [PubMed: 16024513]
13. Gladyshev VN (2014). The Free Radical Theory of Aging Is Dead. Long Live the Damage Theory. Antioxidants Redox Signal. 20, 727–731. 10.1089/ars.2013.5228.
14. Sohal RS, and Weindruch R (1996). Oxidative stress, caloric restriction, and aging. Science 273, 59–63. 10.1126/science.273.5271.59. [PubMed: 8658196]
15. Janssen JAMJL (2021). Hyperinsulinemia and Its Pivotal Role in Aging, Obesity, Type 2 Diabetes, Cardiovascular Disease and Cancer. Int. J. Mol. Sci 22, 7797. 10.3390/ijms22157797. [PubMed: 34360563]
16. Zoncu R, Efeyan A, and Sabatini DM (2011). mTOR: from growth signal integration to cancer, diabetes and ageing. Nat. Rev. Mol. Cell Biol 12, 21–35. 10.1038/nrm3025. [PubMed: 21157483]

17. Jia G, Aroor AR, Martinez-Lemus LA, and Sowers JR (2014). Over-nutrition, mTOR signaling, and cardiovascular diseases. Am. J. Physiol. Regul. Integr. Comp. Physiol 307, R1198–R1206. 10.1152/ajpregu.00262.2014. [PubMed: 25253086]

18. Kenyon CJ (2010). The genetics of ageing. Nature 464, 504–512. 10.1038/nature08980. [PubMed: 20336132]

19. Klass MR (1983). A method for the isolation of longevity mutants in the nematode Caenorhabditis elegans and initial results. Mech. Ageing Dev 22, 279–286. 10.1016/0047-6374(83)90082-9. [PubMed: 6632998]

20. Kenyon C, Chang J, Gensch E, Rudner A, and Tabtiang R (1993). A C. elegans mutant that lives twice as long as wild type. Nature 366, 461–464. 10.1038/366461a0. [PubMed: 8247153]

21. Finch CE, and Ruvkun G (2001). The genetics of aging. Annu. Rev. Genom. Hum. Genet 2, 435–462. 10.1146/annurev.genom.2.1.435.

22. Tullet JMA, Hertweck M, An JH, Baker J, Hwang JY, Liu S, Oliveira RP, Baumeister R, and Blackwell TK (2008). Direct inhibition of the longevity-promoting factor SKN-1 by insulin-like signaling in C. elegans. Cell 132, 1025–1038. 10.1016/j.cell.2008.01.030. [PubMed: 18358814]

23. Ogg S, Paradis S, Gottlieb S, Patterson GI, Lee L, Tissenbaum HA, and Ruvkun G (1997). The Fork head transcription factor DAF-16 transduces insulin-like metabolic and longevity signals in C. elegans. Nature 389, 994–999. 10.1038/40194. [PubMed: 9353126]

24. Hsu A-L, Murphy CT, and Kenyon C (2003). Regulation of aging and age-related disease by DAF-16 and heat-shock factor. Science 300, 1142–1145. 10.1126/science.1083701. [PubMed: 12750521]

25. HUANG J, and MANNING BD (2008). The TSC1–TSC2 complex: a molecular switchboard controlling cell growth. Biochem. J 412, 179–190. 10.1042/BJ20080281. [PubMed: 18466115]

26. Wang C, Wang B, Pandey T, Long Y, Zhang J, Oh F, Sima J, Guo R, Liu Y, Zhang C, et al. (2022). A conserved megaprotein-based molecular bridge critical for lipid trafficking and cold resilience. Nat. Commun 13, 6805. 10.1038/s41467-022-34450-y. [PubMed: 36357390]

27. Pandey T, Zhang J, Wang B, and Ma DK (2023). Bridge-Like Lipid Transfer Proteins (BLTPs) in C. elegans: From Genetics to Structures and Functions. Contact 6, 25152564231186489. 10.1177/25152564231186489.

28. Braschi B, Bruford EA, Cavanagh AT, Neuman SD, and Bashirullah A (2022). The bridge-like lipid transfer protein (BLTP) gene group: introducing new nomenclature based on structural homology indicating shared function. Hum. Genom 16, 66. 10.1186/s40246-022-00439-3.

29. Kane MS, Diamonstein CJ, Hauser N, Deeken JF, Niederhuber JE, and Vilboux T (2019). Endosomal trafficking defects in patient cells with KIAA1109 biallelic variants. Genes Dis. 6, 56–67. 10.1016/j.gendis.2018.12.004. [PubMed: 30906834]

30. Gueneau L, Fish RJ, Shamseldin HE, Voisin N, Tran Mau-Them F, Preiksaitiene E, Monroe GR, Lai A, Putoux A, Allias F, et al. (2018). KIAA1109 Variants Are Associated with a Severe Disorder of Brain Development and Arthrogryposis. Am. J. Hum. Genet 102, 116–132. 10.1016/j.ajhg.2017.12.002. [PubMed: 29290337]

31. Meszarosova AU, Lastuvkova J, Rennerova L, Hitka P, Cihlar F, Seeman P, and Safka Brozkova D (2020). Two novel pathogenic variants in KIAA1109 causing Alkuraya-Kučinskas syndrome in two Czech Roma brothers. Clin. Dysmorphol 29, 197–201. 10.1097/MCD.0000000000000335. [PubMed: 32657846]

32. Murphy CT, Lee S-J, and Kenyon C (2007). Tissue entrainment by feedback regulation of insulin gene expression in the endoderm of Caenorhabditis elegans. Proc. Natl. Acad. Sci. USA 104, 19046–19050. 10.1073/pnas.0709613104. [PubMed: 18025456]

33. Murphy CT, McCarroll SA, Bargmann CI, Fraser A, Kamath RS, Ahringer J, Li H, and Kenyon C (2003). Genes that act downstream of DAF-16 to influence the lifespan of Caenorhabditis elegans. Nature 424, 277–283. 10.1038/nature01789. [PubMed: 12845331]

34. Lee Y, Jung Y, Jeong D-E, Hwang W, Ham S, Park H-EH, Kwon S, Ashraf JM, Murphy CT, and Lee S-JV (2021). Reduced insulin/IGF1 signaling prevents immune aging via ZIP-10/bZIP-mediated feedforward loop. J. Cell Biol 220, e202006174. 10.1083/jcb.202006174. [PubMed: 33666644]

35. Chen Z, Hendricks M, Cornils A, Maier W, Alcedo J, and Zhang Y (2013). Two insulin-like peptides antagonistically regulate aversive olfactory learning in C. elegans. Neuron 77, 572–585. 10.1016/j.neuron.2012.11.025. [PubMed: 23395381]
36. Neve IAA, Sowa JN, Lin C-CJ, Sivaramakrishnan P, Herman C, Ye Y, Han L, and Wang MC (2020). Escherichia coli Metabolite Profiling Leads to the Development of an RNA Interference Strain for Caenorhabditis elegans. G3 (Bethesda) 10, 189–198. 10.1534/g3.119.400741. [PubMed: 31712257]
37. Brooks KK, Liang B, and Watts JL (2009). The Influence of Bacterial Diet on Fat Storage in C. elegans. PLoS One 4, e7545. 10.1371/journal.pone.0007545. [PubMed: 19844570]
38. Taylor SR, Santpere G, Weinreb A, Barrett A, Reilly MB, Xu C, Varol E, Oikonomou P, Glenwinkel L, McWhirter R, et al. (2021). Molecular topography of an entire nervous system. Cell 184, 4329–4347.e23. 10.1016/j.cell.2021.06.023. [PubMed: 34237253]
39. Saltiel AR (2021). Insulin signaling in health and disease. J. Clin. Invest 131, e142241. 10.1172/JCI142241. [PubMed: 33393497]
40. Blackwell TK, Sewell AK, Wu Z, and Han M (2019). TOR Signaling in Caenorhabditis elegans Development, Metabolism, and Aging. Genetics 213, 329–360. 10.1534/genetics.119.302504. [PubMed: 31594908]
41. Thorner J (2022). TOR complex 2 is a master regulator of plasma membrane homeostasis. Biochem. J 479, 1917–1940. 10.1042/BCJ20220388. [PubMed: 36149412]
42. Zhu H, Shen H, Sewell AK, Kniazeva M, and Han M (2013). A novel sphingolipid-TORC1 pathway critically promotes postembryonic development in Caenorhabditis elegans. Elife 2, e00429. 10.7554/eLife.00429. [PubMed: 23705068]
43. Taniguchi M, Kitatani K, Kondo T, Hashimoto-Nishimura M, Asano S, Hayashi A, Mitsutake S, Igarashi Y, Umehara H, Takeya H, et al. (2012). Regulation of autophagy and its associated cell death by “sphingolipid rheostat”: reciprocal role of ceramide and sphingosine 1-phosphate in the mammalian target of rapamycin pathway. J. Biol. Chem 287, 39898–39910. 10.1074/jbc.M112.416552. [PubMed: 23035115]
44. Soukas AA, Kane EA, Carr CE, Melo JA, and Ruvkun G (2009). Rictor/TORC2 regulates fat metabolism, feeding, growth, and life span in Caenorhabditis elegans. Genes Dev. 23, 496–511. 10.1101/gad.1775409. [PubMed: 19240135]
45. Sohrabi S, Cota V, and Murphy CT (2023). Ce Lab, a Microfluidic Platform for the Study of Life History Traits, reveals Metformin and SGK-1 regulation of Longevity and Reproductive Span. Preprint at bioRxiv. 10.1101/2023.01.09.523184.
46. Jones KT, Greer ER, Pearce D, and Ashrafi K (2009). Rictor/TORC2 regulates Caenorhabditis elegans fat storage, body size, and development through sgk-1. PLoS Biol. 7, e60. 10.1371/journal.pbio.1000060. [PubMed: 19260765]
47. Liu P, Gan W, Chin YR, Ogura K, Guo J, Zhang J, Wang B, Blenis J, Cantley LC, Toker A, et al. (2015). PtdIns(3,4,5)P3-dependent Activation of the mTORC2 Kinase Complex. Cancer Discov. 5, 1194–1209. 10.1158/2159-8290.CD-15-0460. [PubMed: 26293922]
48. Calejman CM, Doxsey WG, Fazakerley DJ, and Guertin DA (2022). Integrating adipocyte insulin signaling and metabolism in the multi-omicsera. Trends Biochem. Sci 47, 531–546. 10.1016/j.tibs.2022.02.009. [PubMed: 35304047]
49. Martinez-Lopez N, Mattar P, Toledo M, Bains H, Kalyani M, Aoun ML, Sharma M, McIntire LBJ, Gunther-Cummins L, Macaluso FP, et al. (2023). mTORC2-NDRG1-CDC42 axis couples fasting to mitochondrial fission. Nat. Cell Biol 25, 989–1003. 10.1038/s41556-023-01163-3. [PubMed: 37386153]
50. Heimbucher T, Qi W, and Baumeister R (2020). TORC2-SGK-1 signaling integrates external signals to regulate autophagic turnover of mitochondria via mtROS. Autophagy 16, 1154–1156. 10.1080/15548627.2020.1749368. [PubMed: 32293958]
51. Aspernig H, Heimbucher T, Qi W, Gangurde D, Curic S, Yan Y, Donner von Gromoff E, Baumeister R, and Thien A (2019). Mitochondrial Perturbations Couple mTORC2 to Autophagy in C. elegans. Cell Rep. 29, 1399–1409.e5. 10.1016/j.celrep.2019.09.072. [PubMed: 31693882]

52. Ayuda-Durán B, González-Manzano S, González-Paramás AM, and Santos-Buelga C (2020). Caenorhabditis elegans as a Model Organism to Evaluate the Antioxidant Effects of Phytochemicals. Molecules 25, 3194. 10.3390/molecules25143194. [PubMed: 32668705]
53. Trnka J, Blaikie FH, Smith RAJ, and Murphy MP (2008). A mitochondria-targeted nitroxide is reduced to its hydroxylamine by ubiquinol in mitochondria. Free Radic. Biol. Med 44, 1406–1419. 10.1016/j.freeradbiomed.2007.12.036. [PubMed: 18206669]
54. Chen S, Luo S, Zhang Z, and Ma DK (2019). VHL-1 inactivation and mitochondrial antioxidants rescue C. elegans dopaminergic neurodegeneration. Protein Cell 10, 610–614. 10.1007/s13238-019-0621-4. [PubMed: 30945137]
55. Mangan D (2021). Iron: an underrated factor in aging. Aging (Albany NY) 13, 23407–23415. 10.18632/aging.203612. [PubMed: 34613935]
56. Giorgi C, Marchi S, Simoes ICM, Ren Z, Morciano G, Perrone M, Patalas-Krawczyk P, Borchard S, Jędrak P, Pierzynowska K, et al. (2018). Mitochondria and Reactive Oxygen Species in Aging and Age-Related Diseases. Int. Rev. Cell Mol. Biol 340, 209–344. 10.1016/bs.ircmb.2018.05.006.
57. Goudeau J, Sharp CS, Paw J, Savy L, Leonetti MD, York AG, Up-dike DL, Kenyon C, and Ingaramo M (2021). Split-wrmScarlet and split-sfGFP: tools for faster, easier fluorescent labeling of endogenous proteins in Caenorhabditis elegans. Genetics 217, iyab014. 10.1093/genetics/iyab014. [PubMed: 33693628]
58. Dickinson DJ, and Goldstein B (2016). CRISPR-Based Methods for Caenorhabditis elegans Genome Engineering. Genetics 202, 885–901. 10.1534/genetics.115.182162. [PubMed: 26953268]
59. Jinek M, Chylinski K, Fonfara I, Hauer M, Doudna JA, and Charpentier E (2012). A programmable dual-RNA-guided DNA endonuclease in adaptive bacterial immunity. Science 337, 816–821. 10.1126/science.1225829. [PubMed: 22745249]
60. Tang H, Huang X, and Pang S (2022). Regulation of the lysosome by sphingolipids: Potential role in aging. J. Biol. Chem 298, 102118. 10.1016/j.jbc.2022.102118. [PubMed: 35691340]
61. Trayssac M, Hannun YA, and Obeid LM (2018). Role of sphingolipids in senescence: implication in aging and age-related diseases. J. Clin. Invest 128, 2702–2712. 10.1172/JCI97949. [PubMed: 30108193]
62. Laurila P-P, Wohlwend M, Imamura de Lima T, Luan P, Herzig S, Zanou N, Crisol B, Bou-Sleiman M, Porcu E, Gallart-Ayala H, et al. (2022). Sphingolipids accumulate in aged muscle, and their reduction counteracts sarcopenia. Nat. Aging 2, 1159–1175. 10.1038/s43587-022-00309-6. [PubMed: 37118545]
63. Neuman SD, Levine TP, and Bashirullah A (2022). A novel superfamily of bridge-like lipid transfer proteins. Trends Cell Biol. 32, 962–974. 10.1016/j.tcb.2022.03.011. [PubMed: 35491307]
64. Levine TP (2022). Sequence Analysis and Structural Predictions of Lipid Transfer Bridges in the Repeating Beta Groove (RBG) Superfamily Reveal Past and Present Domain Variations AffectingForm, Function and Interactions of VPS13, ATG2, SHIP164, Hobbit and Tweek, pp. 251525642211343, Contact (Thousand Oaks) 5. 10.1177/25152564221134328.
65. Cutler RG, Thompson KW, Camandola S, Mack KT, and Mattson MP (2014). Sphingolipid metabolism regulates development and lifespan in Caenorhabditis elegans. Mech. Ageing Dev 143–144, 9–18. 10.1016/j.mad.2014.11.002. [PubMed: 25437839]

Highlights

- LPD-3, a megaprotein, regulates insulin-mTOR signaling during *C. elegans* aging
- Agonist insulin INS-7 overproduction in early life shortens *lpd-3* mutants' lifespan
- LPD-3 aids phospholipid trafficking and appropriate balance with sphingolipids
- Hexaceramide abundance, regulated by HYL-1, impacts lifespan via insulin-mTORC2

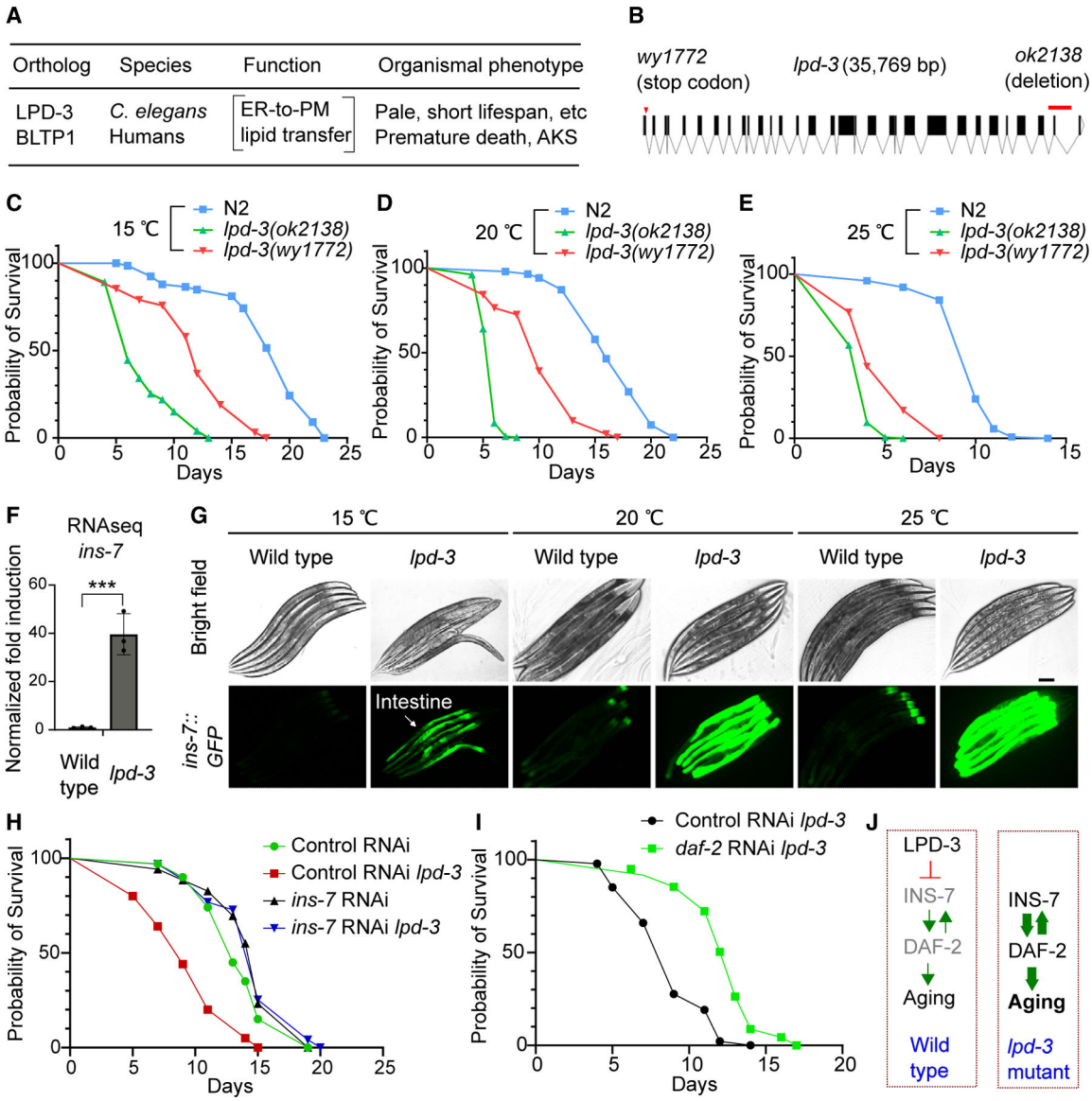

Figure 1. Hyperactivation of ins-7 causes the shortened lifespan in lpd-3 mutants

(A) Cellular function and organismic phenotypes for LPD-3 and the human homolog BLTP1.

(B) Gene diagram showing two alleles of *lpd-3* examined for lifespan phenotypes.

(C) Lifespan analysis of wild type versus *lpd-3* mutants with two different alleles (*ok2138* and *wy1772*) grown at 15°C.($p < 0.0001$, log-rank test).

(D) Lifespan analysis of wild type versus *lpd-3* mutants with two different alleles (*ok2138* and *wy1772*) grown at 20°C.($p < 0.0001$, log-rank test).

(E) Lifespan analysis of wild type versus *lpd-3* mutants with two different alleles (*ok2138* and *wy1772*) grown at 25°C.($p < 0.0001$, log-rank test).

(F) RNA-seq results showing increased *ins-7* expression in *lpd-3* mutants. Values are means ± SD, ***$p < 0.001$ (n = 3 biological replicates).

(G) Representative bright-field and epifluorescence images showing drastically increased *ins-7*p::INS-7::GFP abundance in *lpd-3* mutants. Scale bar, 100 μm.
(H) Lifespan analysis of wild type and *lpd-3*(*ok2138*) mutants with control or *ins-7* RNAi at 20°C, showing the shortened lifespan of *lpd-3*(*ok2138*) rescued by *ins-7* RNAi ($p < 0.0001$, log-rank test).
(I) Lifespan analysis of *lpd-3*(*ok2138*) mutants with control or *daf-2* RNAi at 20°C, showing the shortened lifespan of *lpd-3*(*ok2138*) rescued by *daf-2* RNAi ($p < 0.0001$, log-rank test).
(J) Schematic diagrams illustrating a model of how LPD-3 regulates aging via INS-7 and DAF-2 in wild type and *lpd-3* mutants.

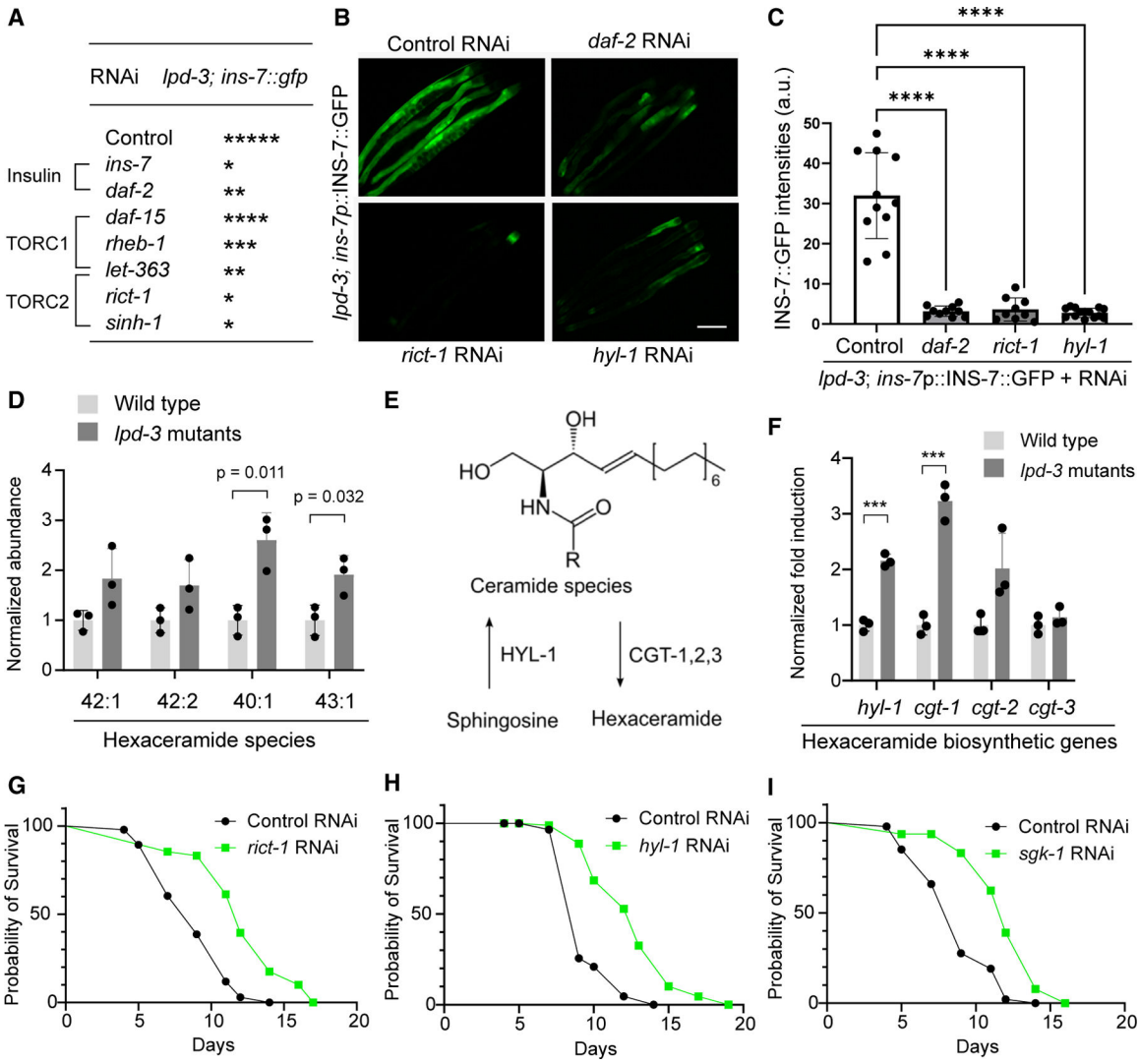

Figure 2. LPD-3 regulates INS-7 via the sphingolipid-ceramide-mTORC2 axis

(A) Table summarizing effects of RNAi against genes in the insulin/mTORC1/mTORC2 pathway on *ins-7*p::INS-7::GFP levels in *lpd-3*(*ok2138*) mutants. The asterisk (*) indicates GFP intensity qualitatively observed under an epifluorescence stereomicroscope.

(B) Representative bright-field and epifluorescence images showing *ins-7*p::INS-7::GFP up-regulation in *lpd-3*(*ok2138*) mutants can be suppressed by RNAi against *daf-2*, *rict-1*, or *hyl-1*. Scale bar, 100 μm.

(C) Quantification of the fluorescence intensities of INS-7::GFP in *lpd-3*(*ok2138*) mutants with indicated RNAi treatment. Values are means ± SD, ****p < 0.0001 (N = 11 animals, one-way ANOVA, Tukey honestly significant difference [HSD] post hoc test).

(D) Lipidomic quantification of hexaceramide species in wild type and *lpd-3*(*ok2138*) mutants. Values are means ± SD (n= 3 biological replicates, two-way ANOVA, Tukey HSD post hoc test).

(E) Schematic showing biosynthetic pathways of hexaceramide, including sphingosine conversion to ceramide by HYL-1 and ceramide to hexaceramide by CGT-1/2/3.

(F) RNA-seq results showing increased *hyl-1* and *cgt-1/2/3* expression in *lpd-3*(*ok2138*) mutants. Values are means ± SD, ***p < 0.001 (n= 3 biological replicates, two-way ANOVA, Tukey HSD post hoc test).
(G) Lifespan analysis of *lpd-3*(*ok2138*) mutants with control or *rict-1* RNAi at 20°C, showing rescued lifespan (p < 0.0001, log-rank test).
(H) Lifespan analysis of *lpd-3*(*ok2138*) mutants with control or *hyl-1* RNAi at 20°C, showing rescued lifespan (p < 0.0001, log-rank test).
(I) Lifespan analysis of *lpd-3*(*ok2138*) mutants with control or *sgk-1* RNAi at 20°C, showing rescued lifespan (p < 0.0001, log-rank test).

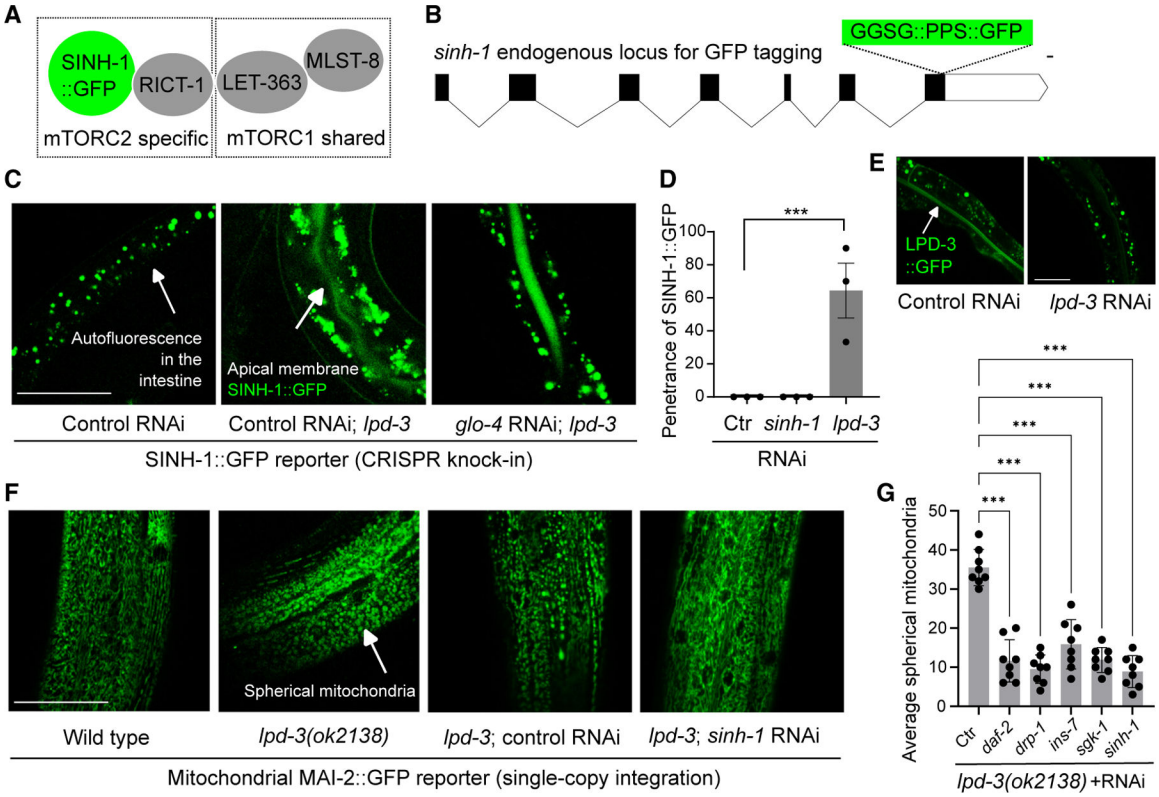

Figure 3. Loss of LPD-3 dysregulates SINH-1/mTORC2 and mitochondria

(A) Schematic showing key components of the mTORC2 complex in the SINH-1::GFP-tagged *C. elegans*.

(B) Schematic gene structure of *sinh-1* showing the CRISPR-mediated knockin allele encoding the endogenous SINH-1 tagged with a linker (GGGS), PreScission Protease site (PPS), and GFP. Scale bar: 100 bp.

(C) Representative z stack confocal fluorescence images showing undetectable SINH-1::GFP signals in animals treated with control but increased SINH-1::GFP enrichment along the apical intestinal membrane in *lpd-3*(*ok2138*) mutants (non-specific gut autofluorescence decreased by *glo-4* RNAi also indicated). Scale bar, 50 μm.

(D) Quantification of the penetrance of SINH-1::GFP enrichment at the apical intestinal membrane in animals with indicated RNAi treatment. Values are means ± SEM, ***p < 0.001 (N = 3 independent experiments, n > 10 in each trial, one-way ANOVA, Tukey HSD post hoc test).

(E) Representative confocal fluorescence images showing decreased LPD-3::GFP by *lpd-3* RNAi. Scale bar, 50 0μm.

(F) Representative confocal fluorescence images showing increased spherical MAI-2::GFP-marked mitochondria in *lpd-3* mutants (day 1) that can be normalized by *sinh-1* but not control RNAi. Scale bar, 50 μm.

(G) Quantification showing rescued mitochondrial morphological defects in *lpd-3*(*ok2138*) mutants by RNAi against genes encoding the mitochondrial fission machinery (*drp-1*) or insulin-mTOR pathway components (e.g., *sinh-1*). Values are means ± SEM, ***p < 0.001 (n = 8 animals per group, one-way ANOVA, Tukey HSD post hoc test).

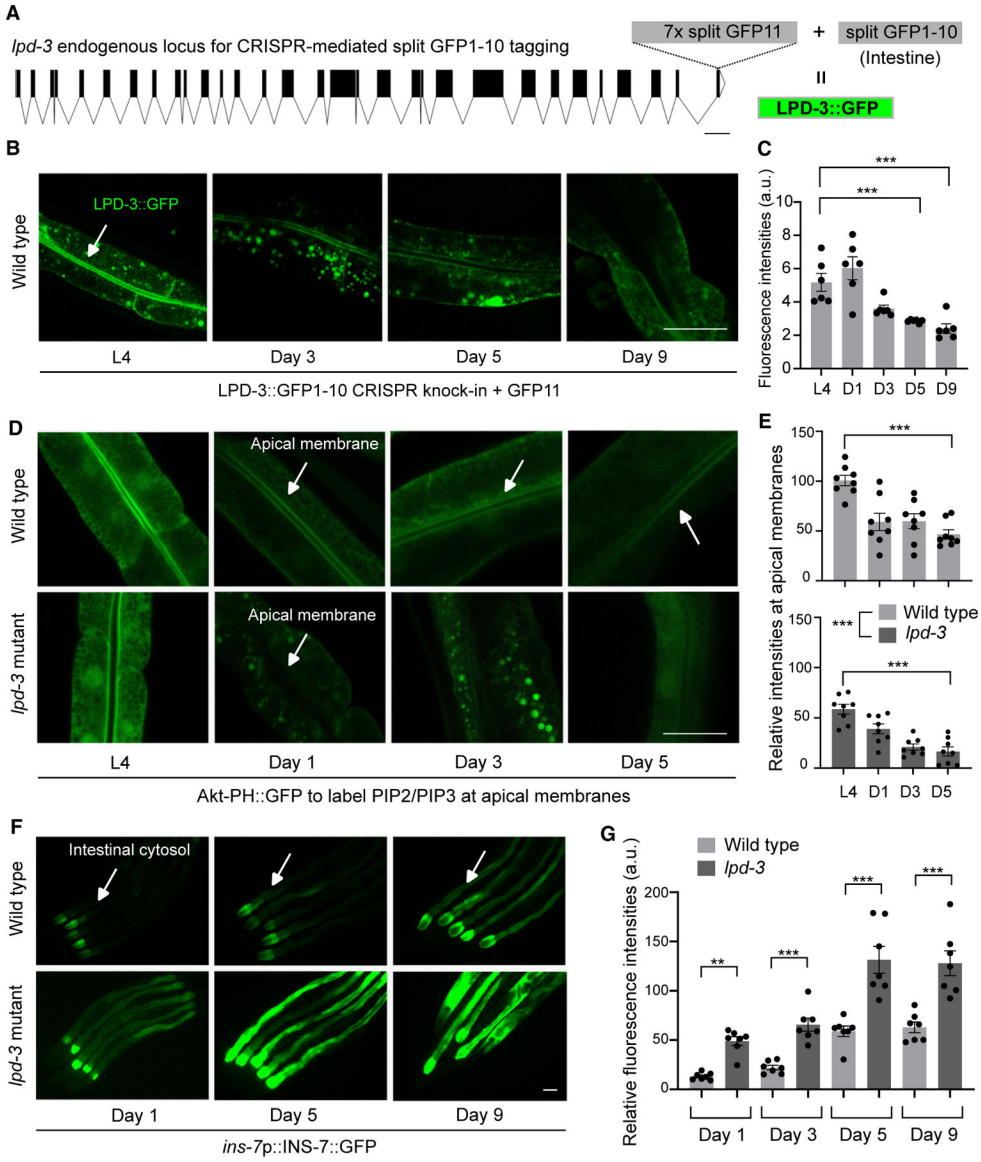

Figure 4. LPD-3 abundance and functions decline with age in wild-type animals

(A) Schematic gene structure of *lpd-3* showing the CRISPR-mediated knockin allele encoding the endogenous LPD-3 tagged with a split GFP1–10 that is complemented by an intestine-expressed GFP11. Scale bar: 500 bp.

(B) Representative confocal fluorescence images showing age-dependent decrease in the abundance of LPD-3::GFP signals in the intestinal apical membrane of animals at the stages of L4 and days 1, 3, 5, and 9 post-L4. Scale bar: 50 μm.

(C) Quantification of the fluorescence intensities of LPD-3::GFP in animals with indicated ages. Values are means ± SEM, ***p < 0.001 (N = 6 biological replicates, one-way ANOVA, Tukey HSD post hoc test).

(D) Representative confocal fluorescence images showing age-dependent decrease in the abundance of Akt-PH::GFP signals that label PIP2/3 in the intestinal apical membrane of

animals at the stages of L4 and days 1, 3, 5, and 9 post-L4 in both wild type and *lpd-3* mutants. Scale bar: 50 μm.

(E) Quantification of the fluorescence intensities of Akt-PH::GFP at apical intestinal membranes in animals with indicated ages. Values are means ± SEM, ***p < 0.001 (N = 8 biological replicates in each stage, N = 32 in each genotype yielding mean fluorescence intensities; one-way ANOVA, Tukey HSD post hoc test).

(F) Representative confocal fluorescence images showing age-dependent increase in the abundance of *ins-7*p::INS-7::GFP signals in animals at the indicated stages in both wild type and *lpd-3* mutants. Scale bar: 50 μm.

(G) Quantification of the fluorescence intensities of *ins-7*p::INS-7::GFP in animals with indicated ages. Values are means ± SEM, with **p < 0.01 and ***p < 0.001 (N = 7 biological replicates, two-way ANOVA, Tukey HSD post hoc test).

KEY RESOURCES TABLE

REAGENT or RESOURCE	SOURCE	IDENTIFIER
Bacterial and virus strains		
Escherichia coli HT115(DE3)	*Caenorhabditis* Genetics Center	N/A
Escherichia coli OP50	*Caenorhabditis* Genetics Center	Wormbase ID: OP50
Ahringer RNAi library	Source BioScience	N/A
Chemicals, peptides, and recombinant proteins		
5-fluoro-2-deoxyuridine	Sigma-Aldrich (St Louis, MO, USA)	50-91-9
Sodium hydroxide	Fisher Scientific (Pittsburg, PA, USA)	1310-73-2
Sodium hypochlorite	Fisher Scientific (Pittsburg, PA, USA)	7681-52-9
Isopropyl-beta-D-thiogalactoside	Fisher Scientific (Pittsburg, PA, USA)	367-93-1
Ampicillin	Sigma-Aldrich (St Louis, MO, USA)	69-53-4
Splash Lipidomix standards	Avanti (Alabaster, AL, USA)	330707-1EA
Methyl *tert*-butyl ether (mTBE)	Sigma-Aldrich (St Louis, MO, USA)	1634-04-4
Hexane	Sigma-Aldrich (St Louis, MO, USA)	110-54-3
Methyl *tert*-butyl ether	Sigma-Aldrich (St Louis, MO, USA)	1634-04-4
Isopropanol	Sigma-Aldrich (St Louis, MO, USA)	67-63-0
Acetonitrile	Sigma-Aldrich (St Louis, MO, USA)	75-05-8
Ammonium acetate	Sigma-Aldrich (St Louis, MO, USA)	631-61-8
FerroOrange	Dojindo (ROCKVILLE, MD, USA)	F374-12
MitoTracker® red CM-H2XRos	Fisher Scientific (Pittsburg, PA, USA)	M46752
Experimental models: Organisms/strains		
N2 Bristol strain (wild type)	CGC	N2
lpd-3(ok2138)	CGC	VC1878
lpd-3(wy1772)	Kang Shen Lab	TV28536
yxIs13 [ins-7p::ins-7::gfp]	Yun Zhang lab in Harvard	ZC1436
yxIs13 [ins-7p::ins-7::gfp]; lpd-3(ok2138)	This study	DMS2205
pwIs890 [Pvha-6::AKT(PH)::GFP]	Barth Grant Lab	RT1619
pwIs890 [Pvha-6::AKT(PH)::GFP]; lpd-3(ok2138)	This study	DMS2122
sinh-1(syb7471[GGSG::PPS::GFP])	Sunybiotech	PHX7471
sinh-1(syb7471[GGSG::PPS::GFP]); lpd-3(ok2138)	This study	DMS2376
lpd-3(wy1770[7xGFP11])	Kang Shen Lab	TV28383
lpd-3(wy1770); wyEx10609	Kang Shen Lab	TV28533
xmSi[mai-2::gfp]	Rosa E. Navarro González Lab	RN80
xmSi[mai-2::gfp]; lpd-3(ok2138)	This study	DMS2089
Oligonucleotides		
daf-2 RNAi	tactgtttgaagacactctgccac	aaactgtgctacacgaaaacgatt
sgk-1 RNAi	atggtgaggaaagatgaggtgaca	tcagaccaaaacgcgattggt
lpd-3 RNAi	ttgacggtctctttgacgtg	actccttgctccgcttgata
Software and algorithms		
PRISM v9	GraphPad Software	RRID:SCR_002798

REAGENT or RESOURCE	SOURCE	IDENTIFIER
MultiQuant software	SCIEX	https://sciex.com/products/software/multiquant-software
ImageJ	NIH	https://imagej.net/ij/index.html
WormLab System	MBF Bioscience	https://www.mbfbioscience.com/products/wormlab-imaging-system